Biochimica et Biophysica Acta 1840 (2014) 2685–2694

Contents lists available at ScienceDirect

Biochimica et Biophysica Acta

journal homepage: www.elsevier.com/locate/bbagen

Mutagenesis and molecular dynamics simulations revealed the chitooligosaccharide entry and exit points for chitinase D from *Serratia proteamaculans*

Jogi Madhuprakash [a,1], Karunakar Tanneeru [b,1], Bhavana Karlapudi [a], Lalitha Guruprasad [b,*], Appa Rao Podile [a,**]

[a] Department of Plant Sciences, School of Life Sciences, University of Hyderabad, Gachibowli, Hyderabad 500046, A.P., India
[b] School of Chemistry, University of Hyderabad, Gachibowli, Hyderabad 500046, A.P., India

ARTICLE INFO

Article history:
Received 19 March 2014
Received in revised form 27 May 2014
Accepted 18 June 2014
Available online 25 June 2014

Keywords:
Chitinases
Chitooligosaccharides
*Sp*ChiD
Transglycosylation
Mutagenesis
Molecular Dynamics Simulations

ABSTRACT

Background: Transglycosylation (TG) activity is a property of glycosyl hydrolases (GHs) with which new glycosidic bonds are introduced between donor and acceptor sugar molecules. This special property of the GHs has potential to generate longer chain chitooligosaccharides (CHOS) that show elicitor activity in plants. We hypothesize that TG activity could be improved by retaining the substrate for a longer duration in the catalytic site.
Methods: Four variants of chitinase D from *Serratia proteamaculans* (*Sp*ChiD) *i.e.* G119S, G119W, W120A and G201W were analyzed in detail for improved TG activity using high performance liquid chromatography (HPLC) and high resolution mass spectrometry (HRMS). The results were strongly supported by 50 ns molecular dynamics (MD) simulations and estimated solvated interaction energies (SIE).
Results: The mutant G119W lost much of both hydrolytic and TG activities, while the mutant G201W displayed increased TG. The trajectory of MD simulations of the mutant G119W showed that the indole rings of two adjacent Trp residues create a major hindrance for the DP4 movement towards the catalytic center. Increased van der Waals (vdW) and coulombic interactions between DP4 substrate and the Trp-201 resulted in enhanced TG activity with the mutant G201W. The average number of hydrogen bonds observed for the DP4 substrate was increased for the mutants G119W and G201W compared to *Sp*ChiD.
Conclusion: The increase in TG activity could be due to partial blocking of product exit of *Sp*ChiD.
General significance: This new approach can be used for generating mutants of GHs with improved TG activity to produce longer chain oligosaccharides.

1. Introduction

Chitinases are a class of glycosyl hydrolases (GHs) that catalyze hydrolysis of β-1, 4 glycosidic bonds present in the homopolymer chitin, made of *N*-acetylglucosamine (GlcNAc) repeating units. Based on sequence similarity, chitinases can be subdivided into two families, 18 and 19 that differ in structure and mode of action [1]. Family 18 chitinases are 'retaining glycoside hydrolases' often found in different organisms, from bacteria to humans [1,2]. Presence of $(\beta/\alpha)_8$ – TIM barrel fold along with several conserved sequence motifs [3] – in the catalytic domain is a characteristic feature of family 18 chitinases [4–8]. The most prominent of these motifs is the DXDXE motif that spans strand 4 of the TIM barrel and includes glutamate that acts as the catalytic acid. The concerted action of two acidic residues, one as general acid-base and the other as nucleophile, results in a reaction with retention of the configuration at the anomeric carbon atom, is known for family 18 chitinases [9]. The substrate-assisted mechanism of the retaining GHs proceeding *via* the formation of a potential oxazoline/oxazolinium ion intermediate was confirmed on the basis of kinetic measurements and crystallographic structures [10–13]. The active site grooves of the retaining chitinases are lined with aromatic amino acids that contribute to substrate binding [6,14].

The overall sequence similarity among family 18 chitinases is not very high. But, an average pairwise identity of 21% (http://www.sanger.ac.uk/Software/Pfam), and occurrence of highly conserved residues in the active site regions with catalytic functions are known [13]. In ChiB of *Serratia marcescens (SmChiB)*, apart from the catalytic twin aspartates Asp-140 & 142 and Glu-144, other amino acids like Tyr-10, Ser-93, Tyr-214, and Asp-215 are well studied. The mechanism of family 18 chitinases is conserved. But, with respect to processive and non-processive, including endo/exo-action, it is conceivable that the active

* Corresponding author. Tel.: +91 40 23134820.
** Corresponding author. Tel.: +91 40 23134503; fax: +91 40 2301 0120.
E-mail addresses: lgpsc@uohyd.ernet.in (L. Guruprasad), arpsl@uohyd.ernet.in (A.R. Podile).
[1] Contributed equally.

http://dx.doi.org/10.1016/j.bbagen.2014.06.014
0304-4165/

site residue flexibility and dynamics are adapted to the variations in the mode of action [10,13,15].

The degradation products of chitin *i.e.*, chitooligosaccharides (CHOS) are gaining special interest due to potential biological applications, especially in the food, medical, and agriculture fields [16,17]. A few of the very important biological activities of CHOS include antibacterial activities [18], antitumor properties [19], antifungal activities [20], and immuno-enhancing effects [21,22]. CHOS regulate the capsular architecture of *Cryptococcus neoformans* cells from both *in vitro* and infected tissues [23]. It was suggested that cellular pathways required for capsule formation and pathogenic mechanisms are affected by blocking chitin-derived structures at the cell surface of *C. neoformans* [23,24]. Thus, targeting CHOS with specific ligands could be a new therapeutic alternative to control cryptococcosis. Despite their biological interest and potential agronomical usefulness, CHOS with well-defined structures remain poorly accessible. Most biological activities require CHOS with a degree of polymerization (DP) ≥ 4 [25]. The synthesis of oligomers with DP ≥ 6 has been a daunting task [26]. Among several methods available for generating CHOS, enzymatic approaches are most promising. Few of the GHs show transglycosylation (TG) activity, forming new glycosidic bonds between donor and acceptor saccharides [26–28]. In retaining GHs, the TG occurs through a double-displacement mechanism [29]. This special property of the GHs can be exploited for the production of not only longer chain CHOS but also well-defined mixtures of CHOS with new or improved biological activity [30], by coupling smaller CHOS building blocks to each other or to other functional groups [27].

The TG activity was improved by chemical modification of residues Trp-62 and Asp-101, at -4 and -2 subsites of hen egg white lysozyme [31] or by mutating a Trp-167 located at subsite -3 of *S. marcescens* chitinase A (*Sm*ChiA) [32]. The Trp-167 was distantly located from the active site *i.e.*, in the chitin-binding cleft. The mutant *Sm*ChiA had improved TG activity with oligosaccharide substrates as well as *p*-nitrophenyl-di-*N*-acetyl-β-D-chitobiose co-incubated with chitotetraose [32]. The variants of Asp-140/311 and Asp-142/313, analogous residues in *Sm*ChiB and *Sm*ChiA, respectively, showed improved TG activity [27]. Alteration of amino acid residues at the catalytic center, catalytic groove, and solvent-accessible region substantially improved the TG activity in chitinase D from *Serratia proteamaculans* (*Sp*ChiD) [33], whereas, the aromatic side chains of Phe-166 and Trp-197, in class V chitinase from *Cycas revoluta* (*Cr*Chi-A), located in the acceptor binding site, were shown to control the TG activity [34] and the introduction of a tryptophan side chain into $+1$ subsite of family GH-18 (class V) chitinase from *Arabidopsis thaliana* (*At*ChiC) enhanced the TG activity [35].

To generate variants of chitinases with improved TG activity, a better understanding of the chitinase-catalyzed hydrolysis and/or TG of CHOS is essential. Introduction of a bulky residue like Trp at '119' and '201' in place of glycine, allowed us to elucidate the CHOS entry and exit points for *Sp*ChiD and unfolded a new possibility to increase the TG activity (Fig. 1). In the present study, the biochemical properties of *Sp*ChiD and its four mutants (G119S, G119W, W120A and G201W) were analyzed by HPLC, High Resolution Mass Spectrometry (HRMS), molecular dynamic (MD) simulations and estimated solvated interaction energies (SIE) free energy were compared to achieve better insights into the mutational effects on hydrolytic and TG activities.

2. Materials and methods

2.1. Bacterial strains, plasmids, culture conditions, biochemicals and enzymes

The plasmid pET-22b (+) and *Escherichia coli* BL21 (DE3) (Novagen, Madison, USA) were used for heterologous expression. *E. coli* was grown in LB broth (1% peptone, 0.5% yeast extract, 1% NaCl) at 37 °C. Ampicillin, at a working concentration of 100 μg/ml, was added to the LB broth as required. Oligonucleotide primers were purchased from Eurofins India (Bangalore, India). Restriction enzymes, T4 DNA ligase and *Pfu* DNA polymerase were obtained from MBI Fermentas (Ontario, Canada). Isopropyl-β-D-thiogalactoside (IPTG), ampicillin and all other chemicals were purchased from Calbiochem or Merck (Darmstadt, Germany). Ni–NTA His bind resin was procured from Novagen (Madison, USA) for protein purification. Different DP CHOS were obtained from Seikagaku Corporation (Tokyo, Japan), through Cape Cod (East Falmouth, USA).

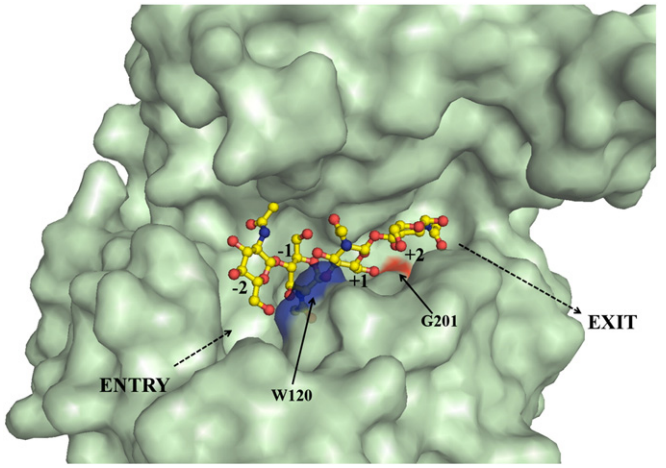

Fig. 1. Surface representation of *Sp*ChiD (PDB code: 4LGX) and the DP4 in the active site represented in the ball and stick (carbon—yellow, nitrogen—blue, oxygen—red). The residues at the probable entry (blue surface—W120) and exit (red surface—G201) sites for the protein *Sp*ChiD were indicated.

2.2. Construction of G119W and G201W mutants

*Sp*ChiD mutants were generated as described by Song-Hua and Madison [36] with pET-22b (+)-*Sp*ChiD as template [26]. Mutagenic primers were designed and followed similar conditions for PCR amplification as described earlier [33]. The primers used for site-directed mutagenesis were 5′-CTGTCCGTCGGT*TGG*TGGGGCGCTCGC-3′ for the Gly119 → Trp mutation (G119W) and 5′-ACCATCGCCGTC*TGG*GCCAAC GTGAAA-3′ for the Gly201 → Trp mutation (G201W) (the mutation sites are italicized and underlined). Each mutation was introduced into pET-22b (+)-*Sp*ChiD the inserted mutation was confirmed by automated DNA sequencing (Eurofins, Bangalore, India). The constructs, with desired mutations were transformed into *E. coli* BL21 (DE3) for protein over expression.

2.3. Protein expression, isolation and purification

Expression of *Sp*ChiD and the mutant proteins was done as described by Neeraja et al. [37]. The harvested culture pellet was processed for isolation of periplasmic fraction (PF) as described in pET manual (Novagen, Darmstadt, Germany). The PFs with desired proteins were purified as described in Qiagen (Duesseldorf, Germany) manual using Ni-NTA affinity chromatography under native conditions. The recombinant protein bound to the Ni-NTA matrix was eluted with different concentrations of imidazole containing buffers [33]. The purified fractions were electrophoresed on 12% SDS-PAGE and visualized using Coomassie brilliant blue. Fractions with high purity were selected for concentration and buffer exchanged with 20 mM sodium acetate, pH 5.6, using amicon filters of 10 kDa cut-off (Millipore, Billerica, MA).

2.4. Chromatography of CHOS generated by the mutants G119W and G201W

HPLC analysis was done to check the mutational effects on hydrolytic and TG activities of G119W and G201W mutants of *Sp*ChiD. Two mM chitotetraose (DP4) was taken as the starting substrate and incubated with 350 nM of the purified glycine variants. All the experimental parameters were kept unchanged to make a comparative study with

*Sp*ChiD and the mutants G119S and W120A, which were reported and described in Madhuprakash et al. [33]. In brief, the reaction was performed in 20 mM sodium acetate buffer, pH 5.6, at 40 °C and the CHOS fractions collected at different time intervals (up to 6 h) were separated by normal-phase HPLC using 70% acetonitrile on SHODEX Amino-P50 4E column (4.6 × 250 mm ID, Showa Denko K.K., USA). Flow rate of 0.7 ml/min was maintained and eluted CHOS were monitored at 210 nm. The values of initial decrease in DP4 concentration were considered for specific activity measurements through linear regression analysis using OriginPro 8 software.

2.5. Product analysis by HRMS

The reaction products of *Sp*ChiD and the mutants G119S, G119W, W120A and G201W were analyzed using BRUKER maXis high resolution mass spectrometry (HRMS). Fractions collected at 30 min for *Sp*ChiD and 6 h for the mutants G119S, G119W, and G201W were used for HRMS analysis. High resolution mass spectra were recorded on micromass ESI-TOF-MS under low positive ion mode and the complete acquisition parameters are mentioned in the supplemental information.

2.6. MD simulations

The *Sp*ChiD homology model with DP4 substrate [33] was adopted. Point mutations G119S, G119W, W120A and G201W were generated by using "build mutant" module under protein modeling protocol implemented in Discovery Studio 2.5. The *Sp*ChiD and its four variants in complex with DP4 substrate were subjected to MD simulations for 50 nanoseconds (ns) at constant temperature and pressure in a periodic cubic box with an edge length of approximately 1.5 nm. In addition, we also performed MD simulations for the 'apo' form of *Sp*ChiD crystal structure (PDB_ID: 4LGX) which was solved very recently [38]. We used the AMBER ff99SB force field for the protein. The ligand parameter files with the AMBER ff99SB and GAFF force fields using antechamber [39,40] were generated, with ACPYPE script [41]. All the simulations were performed by using GROMACS 4.5.5 software [42,43]. The protein was solvated in the cubic box using explicit solvent-SPC model water molecules around the *Sp*ChiD–DP4 complex structure. The charge of the protein complex was neutralized using three chloride ions. During MD simulations, we initially performed 5000 steps of steepest descent minimization and 1 ns position restrained dynamics to distribute water molecules throughout the system. Finally, we performed MD simulations of the whole system for 50 ns, using 0.002 ps time step. The Particle Mesh Ewald (PME) summation method [44,45] was employed for calculation of electrostatics, with a real space cut-off of 10 Å, PME order of 6 and a relative tolerance between long- and short-range energies of 10^{-6}. Short range interactions were evaluated using a neighbor list of 10 Å updated every 10 steps. The Lennard–Jones (LJ) interactions and the real space electrostatic interactions were truncated at 9 Å. The V-rescale thermostat [46] and Parrinello–Rahman algorithm [47] were used to maintain temperature and pressure of 1 atm, respectively, whereas, hydrogen bonds were constrained using LINCS algorithm [48]. The last 5 ns of trajectory file obtained from the MD simulations was used for generation of the average structure. The average structure was minimized for 2500 steps of steepest descent minimization and 1000 steps of conjugate gradient method to get energy minimized average structure. From this energy minimized average structure, the interactions between *Sp*ChiD and its mutant complexes were observed. Results were analyzed using Grace for XY plots, VMD and Discovery Studio 2.5 visualizer for trajectory visualizations.

2.7. Solvated interaction energies

SIE free energies were calculated using parameters that have been fitted to reproduce binding free energies of a data set of 99 protein–ligand complexes [49,50]. It is an end-point physics-based, force-field-based scoring function for predicting ligand-binding affinities. This approximation of binding free energy in solution resembles the formalism used in other physics-based binding free energy end-point calculation methods, including Molecular Mechanics–Poisson Boltzmann/Generalized Born Surface Area (MM–PB (GB)/SA) [51–54] and Linear Interaction Energy (LIE) [55]. Binding free energies (ΔG) for the protein–ligand complexes were estimated using the SIETRAJ program [49,56]. SIETRAJ (http://www.bri.nrc.ca/ccb/pub) is an alternative to the MM–PBSA software provided by the AMBER distribution. It is a set of scripts and executables for carrying out the SIE calculation on molecular dynamics trajectory or a single snapshot of target–ligand complex. This program calculates ΔG for snapshot structures from the MD simulations with a rigid infinite separation of protein and ligand [49]. ΔG is the sum of intermolecular van der Waals (vdW), coulomb interactions, change in reaction field energy (determined by solving the Poisson–Boltzmann equation) and non-polar solvation energy (proportional to the solvent-accessible surface area) [49]. Similar to MMPBSA/GBSA, SIE treats the protein ligand system in atomistic detail and solvation effects implicitly. The free energy of binding between ligand and protein is computed by:

$$\Delta G_{bind}(\rho, D_{in}, \alpha, \gamma, C) = \alpha[\Delta E_{vdW} + \Delta E_{Coul}(D_{in}) + \Delta G_{RF}(\rho,\ D_{in}) + \gamma \Delta SA(\rho)]\ + C$$

where, ΔE_{vdW} and ΔE_{Coul} are the intermolecular vdW and coulomb interaction energies between protein and ligand. ΔG_{RF} (ρ, D_{in}) is the difference in reaction-field energy between the bound and free states of protein ligand complex as calculated by solving the Poisson equation with BRIBEM [57–59]. ΔSA (ρ) is the difference in molecular surface area between the bound and free states of protein. The default values of the parameters are: $\rho = 1.1$, $D_{in} = 2.25$, $\gamma = 0.0129$ kcal/(mol^3 A^2), $C = -2.89$ kcal/mol, and $\alpha = 0.1048$. Where 'ρ' is the linear scaling factor of the vdW radii of the AMBER99 force field, D_{in} is solute interior dielectric constant, 'γ' is the molecular surface tension co-efficient describing the non-polar component of solvation free energy, 'α' is the pre-factor that implicitly quantifies the loss of entropy upon binding, and 'C' is the constant that includes protein-dependent contributions not explicitly modeled by the SIE methodology. The scaling can be considered a crude treatment of entropy–enthalpy compensation containing the caveats of implicit solvation and neglecting the vibrational entropy [49,60]. Here, we estimated ΔG by averaging 500 structures from the 50 ns of selected MD snapshots and averaging over the resulting free energies obtained from each snapshot.

3. Results

3.1. Hydrolytic & TG activities of the mutants G119W and G201W compared against SpChiD

HPLC chromatogram (Fig. 2A) and the quantification profile (Fig. 2B) of wild type *Sp*ChiD were taken from Madhuprakash et al. [33], for clear comparison of hydrolytic and TG activities with the mutants G119W and G201W. Gly119 → Trp conversion resulted in a substantial decrease of both hydrolytic and TG activities. A much smaller quantity of degradation products was detected at '0' min with a proportion of 0.4, 0.2 and 0.8% of DP1, DP2 and DP3, respectively. No TG activity was detectable up to 15 min (Fig. 2C). The quantifiable TG products like DP5 and DP6 were detected from 20th min. A marginal increase of hydrolytic (DP1-DP3 with a proportion of 1.0, 0.7, and 1.1%, respectively) and TG (DP5 and DP6 with a proportion of 0.4 and 0.3%) products were observed at 30 min (Fig. 2D). Though there was a considerable decrease in the initial DP4 substrate concentration to 94.4% at 90 min, the increase in proportion of TG products was much less. A similar effect was observed at the end of 6 h with accumulation of quantifiable oligomers from DP1-DP6 in a proportion of 1.1, 1.6, 1.7, 93.6, 0.8 and 1.1%, respectively.

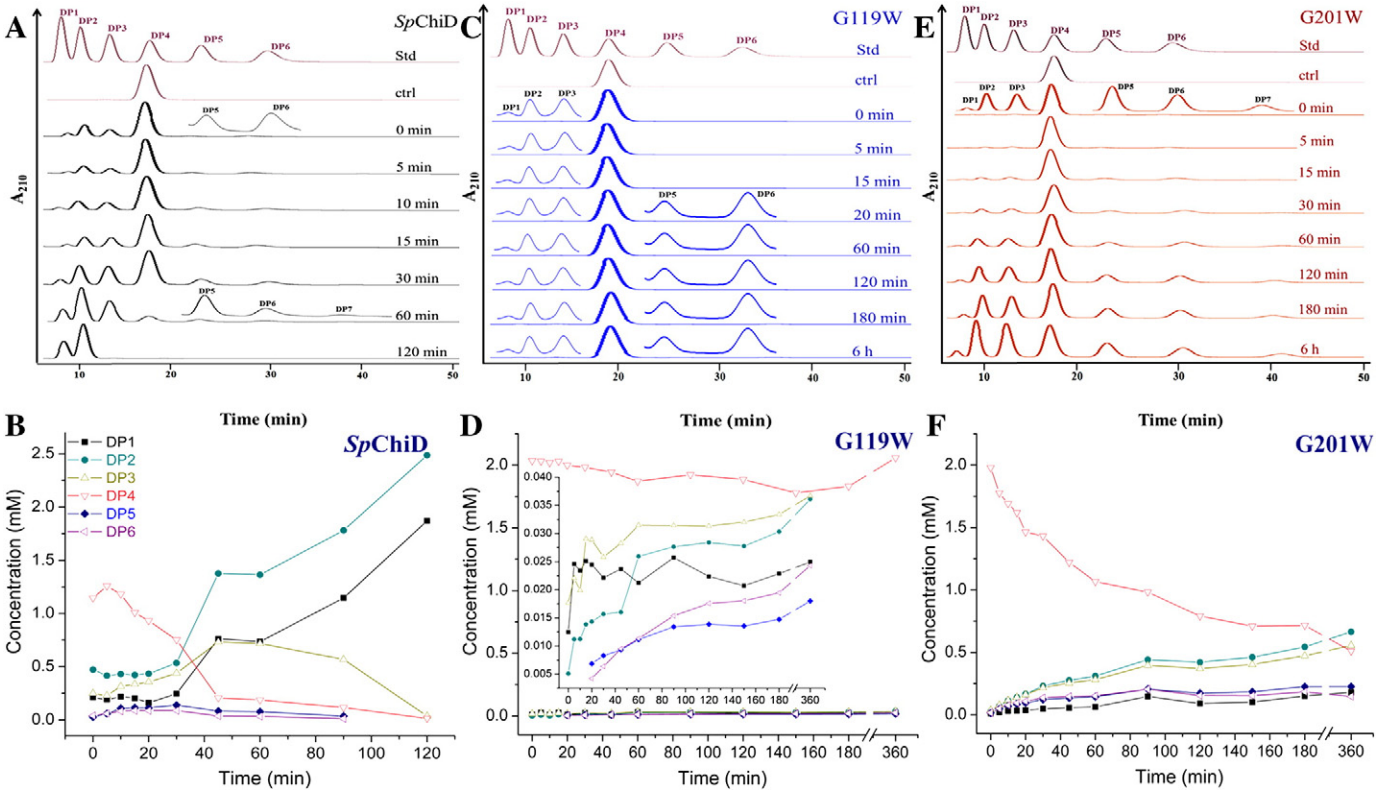

Fig. 2. Product profiles of *Sp*ChiD [33] and the mutants G119W and G201W. A, C and E are the HPLC chromatograms and B, D and F are the quantification profiles for the mutants G119W and G201W, respectively. In each chromatogram the topmost profile shows a standard mixture of CHOS ranging from DP1-DP6. In A, C & E the insets show the magnified view of the low peak area products present at regular time intervals. Control represents the substrate without the enzyme treatment. Individual quantification graph represents all the hydrolytic (DP1–DP3) and TG (DP5, DP6) products accumulated during the course of reaction. Since the mutant G119W had much less activity, to highlight the reaction products in the quantification profile of G119W, inset showing both hydrolytic and TG products was given for D. The symbols used in B, D & F are the same and represented as inset in B.

The quantification profile of mutant G201W showed a gradual decrease of DP4 substrate concentration through time (Fig. 2E). The TG products DP5 and DP6 with a proportion of 0.7% and 0.8%, respectively accumulated at '0' min. At 30 min the relative percentage of TG products increased to 5.6 (DP5) and 6.3 (DP6). More than half of the initial DP4 substrate was depleted (41.3%) by 90 min with similar quantities (8.6%) of both the TG products retained. At the end of 6 h the proportion of DP6 decreased to 6.4%, and the DP5 increased to 9.9%, whereas, the hydrolytic products like DP1–DP3 were observed in a proportion of 7.9, 29.1 and 24.3%, respectively, with only 22.3% of DP4 left at the end of 6 h (Fig. 2F). DP2 was the major end product formed with the mutant G201W. The relative percentage of specific activity (Supplementary Fig. 1) and TG activity of the mutants G119W and G201W were compared against *Sp*ChiD and its two other variants G119S and W120A (Table 1). HRMS data confirmed the presence of both hydrolytic and TG products for *Sp*ChiD and its mutants G119S, G119W, W120A and G201W (data given as supplementary information).

Table 1
Relative specific activity and TG activity of *Sp*ChiD and its mutants towards DP4 substrate. +" indicates minimum; −" indicates nil; +++" indicates high.

Name of the enzyme	Relative % of specific activity	Relative TG activity
*Sp*ChiD	100	+
G119S	72.8	+++
G119W	11.2	−
W120A	830.6	−
G201W	113.6	+++

3.2. MD simulations

A multiple sequence alignment of several representative GH-18 family proteins showed that the length of proteins is variable. However, the active site of these proteins showed high degree of conservation with few substitutions and occasional deletions/insertions (data not shown), suggesting that the fold and function of GH-18 family proteins is highly conserved. To elucidate the role of amino acid residues interacting with DP4 substrate in the *Sp*ChiD tunnel, we performed five separate 50 ns MD simulations for the *Sp*ChiD and the four individual mutants (W120A, G119S, G119W and G201W) in complex with DP4. The residues showing major interactions with the DP4 substrate in the active site of four *Sp*ChiD mutants are shown in Fig. 3A–D. The residues F-64 (−2 subsite); Y-331 and W-401 (−1 subsite) are positioned at the tunnel entrance side of *Sp*ChiD. The residue W-166 is located in the extended loop region of the DXDXE motif and blocking the tunnel from +1 subsite.

In the present study, the residues G-119, W-120 and G-201 are targeted and studied in detail. From the simulations, we calculated the root mean square deviation (RMSD) of the homology model complexes and 'apo' form of *Sp*ChiD crystal structure (Supplementary Figs. 2 and 3). Superimposition of 10 structures taken at every 5 ns interval revealed that the alterations were only in the loop conformations while retaining the protein core during the MD simulations. These conformations in the 'apo' form of *Sp*ChiD crystal structure are shown in Supplementary Fig. 4.

The root mean square fluctuation (RMSF) plots shown in Fig. 4, of all the four mutants were compared with the *Sp*ChiD, which revealed the site-specific fluctuations in the protein during the MD simulations.

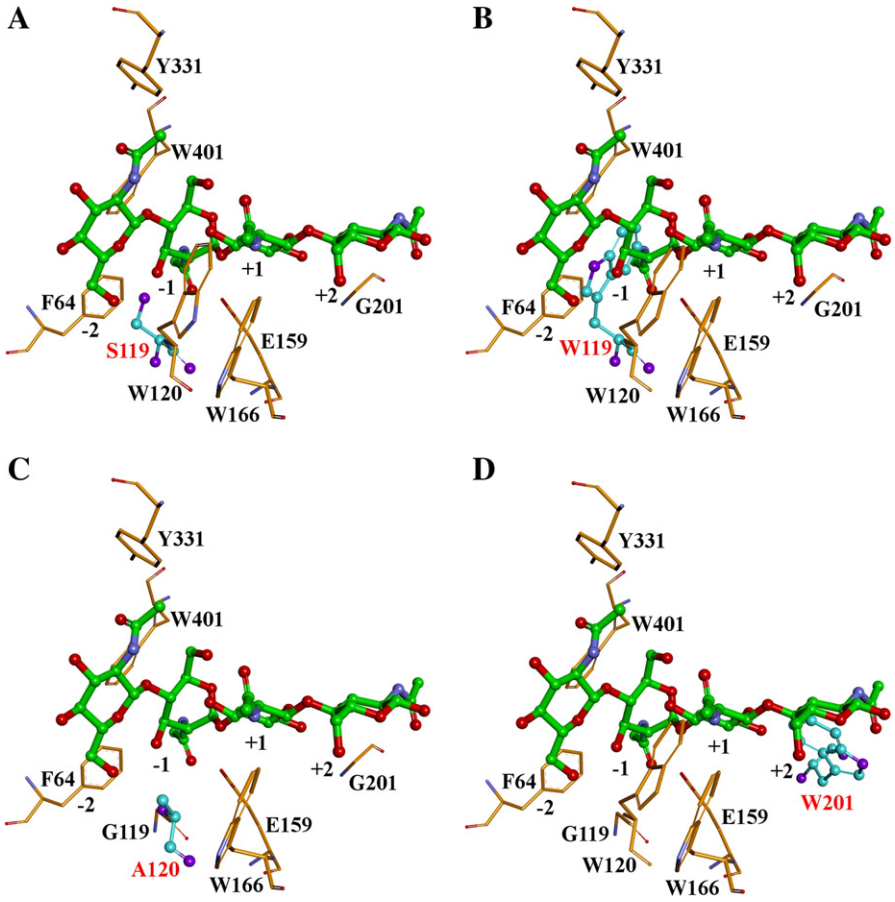

Fig. 3. The *Sp*ChiD (PDB code: 4LGX) mutants with DP4 in the active site. The important active site residue side chains are shown in the stick model. The DP4 represented in ball and sticks model with green—carbons, red—oxygen, blue—nitrogen. The mutants (A) G119S (B) G119W (C) W120A (D) G201W are shown in ball and stick model with cyan—carbons and purple—oxygens, nitrogens.

*Sp*ChiD showed greater fluctuations at the residue segment in the chitin path 86–95 that affect the binding of the chitin towards the active site. The extended loop regions (292–300 and 311–325) of the β7 strand of the TIM barrel also showed greater fluctuations. But, these regions were observed far from the chitin binding site. The overall RMSF of the protein was restricted to ~0.08 nm indicating that the protein

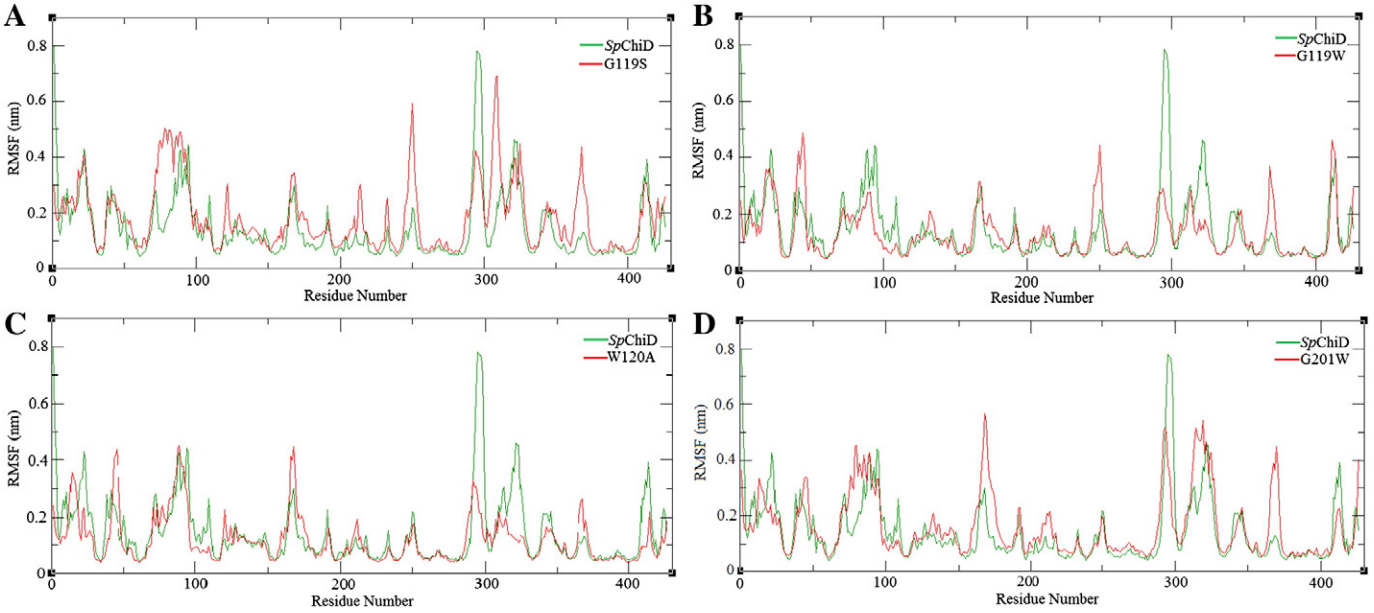

Fig. 4. Root mean square fluctuation plots from 50,000 ps MD simulations of the *Sp*ChiD and its four mutants: A) G119S; B) G119W; C) W120A; and D) G201W. *Sp*ChiD is represented in green and the mutants are represented in red.

remained stable. The other loop regions of the protein also displayed minor fluctuations during the simulations.

The mutant G119S also showed increased RMS fluctuations in specific regions compared to *Sp*ChiD (Fig. 4A). The helix region next to the β2 strand of the TIM barrel (71–94) near the active site and the loop region next to the β6 of the TIM barrel (247–251) had greater fluctuations. In addition, the regions 305–310, next to β7, and the region 365–370 between the β10 and β11 strands also showed greater fluctuations than *Sp*ChiD. The mutant G119W showed less fluctuations compared to G119S with that of *Sp*ChiD. Further, the region 40–44 between β1 and β2 which was in the path of chitin, the region next to β6 (245–251) and the region next to β7 strand (368–369) showed increased fluctuations compared to *Sp*ChiD (Fig. 4B). The other regions displayed minimal differences from *Sp*ChiD.

In comparison with the *Sp*ChiD, W120A mutant (Fig. 4C) exhibited decreased RMS fluctuations in most of the regions. The region 165–170, that corresponds to the extended loop region from the DXDXE motif, had more fluctuations than the *Sp*ChiD. The loop region between β10 and β11, which is far from the active site, also had more fluctuations than the *Sp*ChiD. The mutant G201W showed slightly higher fluctuations than the *Sp*ChiD. A broad region corresponding to the segment next to the β2 strand of the TIM barrel (75–94) and the extended loop region (165–170) from the DXDXE motif showed increased fluctuations (Fig. 4D). The residues in the helix region (311–325), observed next to the β7 strand and the region 365–370 between the β10 and β11 strands, displayed increased fluctuations.

3.3. SIE free energy calculations

We have calculated SIE free energies for the *Sp*ChiD and four mutants from the 50 ns of MD simulations. The intermolecular vdW, coulombic energies, the change in surface area and ΔG are shown in Supplementary Table 1. The *Sp*ChiD with DP4 substrate showed a ΔG of −10.66 kcal/mol indicating good binding of protein–ligand complex. The other four mutants showed less binding in comparison with *Sp*ChiD. The two mutants G119S (−10.32 kcal/mol) and G119W (−10.50 kcal/mol) showed similar binding free energies with DP4. The other two mutant complexes of W120A and G201W had less SIE binding free energies, −9.41 kcal/mol and −9.84 kcal/mol, respectively. To understand the importance of the selected residues like Trp-120, Gly-119 and Gly-201 in substrate binding, their contribution in binding free energies was determined both in the native and mutant forms of *Sp*ChiD. The efficient contributions to the binding free energies of DP4 by the selected mutants are listed in Table 2. The mutant residue Ala-120 showed decreased vdW (−0.74 kcal/mol) and coulombic (−0.13 kcal/mol) energies in comparison to Trp-120 in the native form of *Sp*ChiD–DP4 complex (vdW = −2.46 kcal/mol, coulomb = −0.78 kcal/mol). The other two residues in the W120A mutant (in complex with DP4 substrate), Gly-119 with decreased energies and Gly-201 with slightly increased vdW and coulomb energies were observed compared to native *Sp*ChiD–DP4 complex. For the G119S–DP4 complex, the mutant residue Ser-119 showed much less vdW (−0.35 kcal/mol) and coulomb (0.01 kcal/mol) energy contributions in comparison to *Sp*ChiD–DP4 complex (vdW = −1.40 kcal/mol, coulomb = −0.86 kcal/mol). In the mutant complex G119S–DP4, the residue Trp-120 showed decreased energy contributions whereas, Gly-201 was observed with slightly increased vdW and coulombic energies. For the G119W-DP4 complex, the mutant residue Trp-119 experienced a very high vdW (−4.77 kcal/mol) and coulombic (−1.31 kcal/mol) energies than the *Sp*ChiD–DP4 complex. The other two residues Trp-120 and Gly-201 displayed decreased vdW and coulombic energy contributions, in comparison to *Sp*ChiD–DP4 complex. In the G201W–DP4 mutant complex, the Trp-201 showed very high vdW (−3.91 kcal/mol) and coulombic (−3.85 kcal/mol) energies in comparison to *Sp*ChiD–DP4 complex. The two residues Trp-120 and Gly-119 experienced decreased vdW and coulombic energies compared to the same residues from *Sp*ChiD–DP4 complex.

The hydrogen bonding analysis of DP4 substrate in the active site of *Sp*ChiD and the four mutants during 50 ns of MD simulations allowed us to measure the binding efficiency of the ligand. Alteration in the number of hydrogen bonds in the enzyme–substrate complexes revealed the effect of specific mutation on the binding efficiency of substrate. The average number of hydrogen bonds observed for DP4 substrate during the 50 ns of MD simulations with mutants G119S, G119W, G201W, W120A and *Sp*ChiD are 5.8, 9.4, 7.2, 5.6 and 5.6, respectively. The number of hydrogen bonds for *Sp*ChiD and mutant–DP4 complexes is shown in the Fig. 5.

Table 2
The van der Waals (vdW) and coulombic (coulomb) interaction energy contribution to SIE binding free energy of DP4 with *Sp*ChiD and its mutants from selected binding site residues.

Name of protein	Residue number	vdW (kcal/mol)	Coulomb (kcal/mol)
*Sp*ChiD	Trp120	−2.46	−0.78
	Gly119	−1.40	−0.86
	Gly201	−0.47	−0.25
W120A	Ala120	−0.74	−0.13
	Gly119	−0.65	−0.33
	Gly201	−0.89	−0.28
G119S	Trp120	−0.57	−0.04
	Ser119	−0.35	0.01
	Gly201	−0.69	−0.33
G119W	Trp120	−2.40	−0.58
	Trp119	−4.77	−1.31
	Gly201	−0.74	−0.27
G201W	Trp120	−0.79	−0.04
	Gly119	−0.09	0.21
	Trp201	−3.91	−3.85

4. Discussion

To understand the biochemical properties of carbohydrate active enzymes, more detailed investigations are needed on the protein–carbohydrate interactions. A majority of these interactions are accomplished by the aromatic amino acids like tryptophan, tyrosine, and phenylalanine, wherein aromatic rings can stack against planar faces of carbohydrate rings *via* carbohydrate–π interactions [33,61]. GHs are ubiquitous in nature and typically exhibit tunnels, clefts, or pockets lined with aromatic residues for processing carbohydrates. Removal of aromatic residues at the entrance and exit of the *Trichoderma reesei* family 6 cellulase (Cel6A) tunnel dramatically impacted the binding affinity, suggesting that these residues play a role in chain acquisition and product stabilization, respectively [61].

Structural studies on chitinases from *S. marcescens*, *Sm*ChiA [4] and *Sm*ChiB [62] revealed deep substrate-binding clefts, due to the presence of a 70–90 residue insertion in the catalytic domain ('α + β domain'), which is absent in other chitinases such as hevamine [5] and *Sm*ChiC [15]. Both *Sm*ChiA and *Sm*ChiB contain an additional substrate-binding domain, which extends the substrate-binding cleft on the side where the non-reducing end of the substrate binds in *Sm*ChiA [4] and on the side where the reducing end of the substrate binds in *Sm*ChiB. [62] On the basis of structural characteristics [4,62] and enzymological work [14,63] it was suggested that *Sm*ChiA and *Sm*ChiB are exo-chitinases, which degrade chitin chains from opposite ends [64]. In an alternative approach, the end specificity of *Sm*ChiA and *Sm*ChiB was experimentally demonstrated. Hult et al. [65] used a combined analysis of tilt micro-diffraction method to determine the crystallographic axes and the BXH–SG (biotinamidocaproyl hydrazide–streptavidin–gold) labeling method specific to the reducing ends of the enzymatically degraded β-chitin microcrystals.

Mutational studies at the catalytic groove of *Sp*ChiD revealed the possibilities to improve TG activity. Four out of five different mutations (F64W, S116G, G119S and F125A) displayed increased TG activity [33],

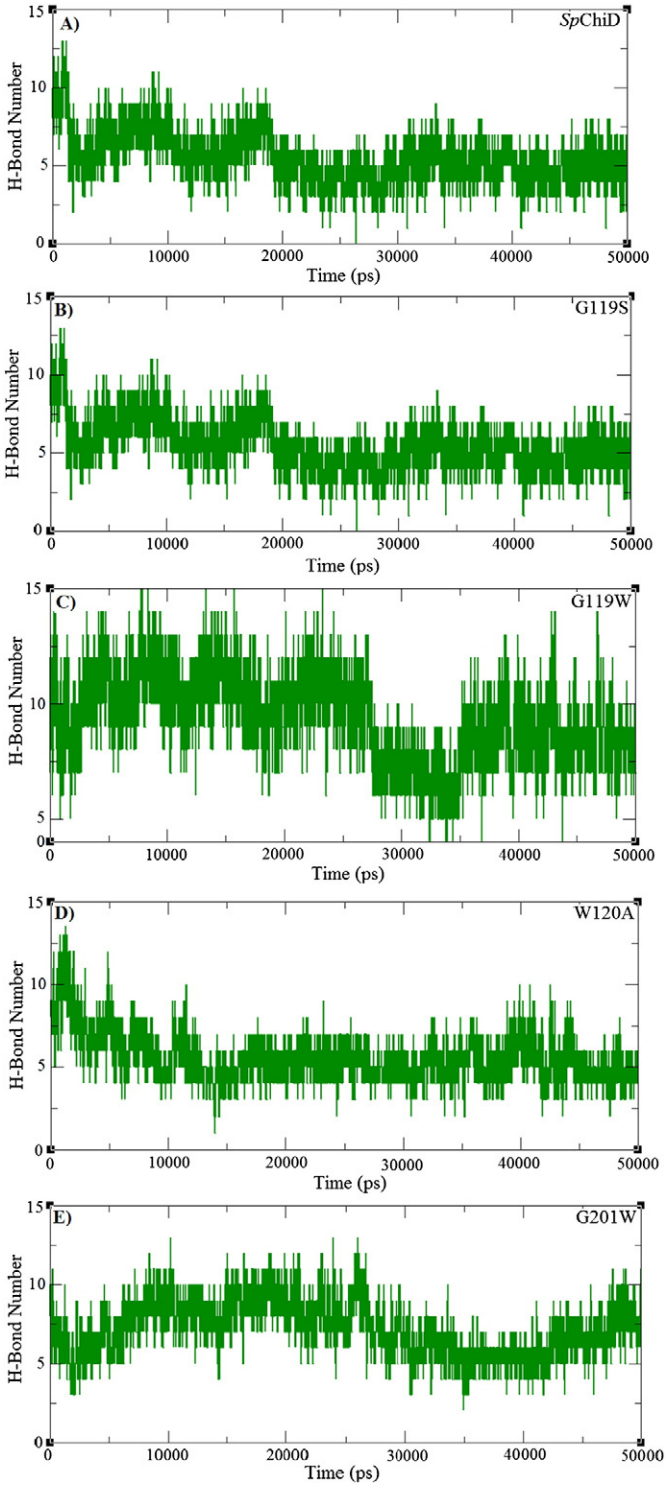

Fig. 5. Number of hydrogen bonds (green) formed during the 50,000 ps of MD simulations by DP4 with A) *Sp*ChiD, B) G119S, C) G119W, D) W120A, and E) G201W.

suggesting that this region could be the entry site of CHOS for *Sp*ChiD. Other side of the groove was occupied primarily by the residues Asn-203, Lys-205, Met-230, Tyr-232 and Tyr-256 where only Gly-201 can be mutated to bulky Trp for partial blocking of product exit. Here, we measured the possible variations in the interactions of specific amino acid residues of *Sp*ChiD with DP4 substrate. We also determined the substrate entry and product exit points for the enzyme *Sp*ChiD and showed that partial blocking of the product exit enhanced the TG activity.

Interactions displayed by the aromatic amino acid side-chains with the planar faces of carbohydrates are typical signature motifs [66]. In agreement with this, we mutated two glycine residues to corresponding tryptophans, on either side of the *Sp*ChiD tunnel. In the native *Sp*ChiD, glycine and tryptophan are present at positions '119' and '120', respectively. The residue region 119–120 was considered as the probable substrate entry point. Detailed analysis of the β-α3 loop in ChiC, from *S. marcescens* (residues 102–114) revealed the presence of a conserved sequence motif SXGG (from residues 102–105) in GH18 chitinases. This conserved motif is usually followed by a Trp in processive chitinases (in ChiA and ChiB: S*I*GGW), which is vital for processivity and the ability to efficiently degrade insoluble chitin [15]. In *Sp*ChiD, the S*X*GG motif corresponds to 116–119 region and the Gly-119 targeted is from the motif itself, followed by Trp at 120th position which is a characteristic feature of processive chitinases [15,67]. The residues Gly-119 and Trp-120 were present on the β3 strand of TIM barrel closer to the catalytic center. Both these residues were thought to maintain the architecture of the catalytic groove and to a major extent maintained by Trp-120 with its bulky side chain. Mutation of Trp-120 to Ala in *Sp*ChiD resulted in a substantial loss of TG activity and increased hydrolysis [33] whereas, change of Gly-119 to Ser resulted in increased TG activity. The pre-existing stacking interactions of Trp-120 with the substrate, which further increased with the adjacent Ser-OH group, might contribute to increased TG activity [33].

In the present study, Gly-119 was mutated to Trp, which resulted in the loss of both hydrolytic and TG activities to a greater extent. The involvement of Trp-119 in binding to the DP4 substrate was assessed through MD simulations and SIE studies. The very high and increased vdW and coulombic interaction energies (Table 2) indicate not only the side chain of Trp-119 experienced closer interactions with the DP4 substrate but also retained the interactions with Trp-120. From the trajectory of MD simulations, we also observed that the side chains of these two residues are blocking the tunnel entrance to a major extent. The RMSD of DP4 substrate was stabilized at 0.22 nm in the active site and showed better interactions with the Trp-119 residue (Supplementary Fig. 2), in turn, restricting the movement of the substrate within the active site. The average number of hydrogen bonds also increased in comparison to the *Sp*ChiD–DP4 complex during MD simulations for mutant G119W. The loss of hydrolytic and TG activities to a greater extent may be due to the major hindrance caused by abutting bulky side chains of Trp (positions 119 and 120) at the tunnel entrance and allowed only a few substrate molecules to reach the active site. The soluble substrates like CHOS could enter the substrate binding cleft from various directions [68], possibly contributed to the feeble activity displayed by the mutant G119W. Commencement of TG activity at 20 min and its very little increase up to 6 h in terms of quantifiable TG products was plotted and compared against *Sp*ChiD and three other single mutants (Fig. 6). The concentration of quantifiable TG products, DP5 and DP6 remained similar till the end of 6 h. The major loss of both hydrolytic and TG activities for the mutant G119W supports the assumption that Gly-119 is part of substrate entry site for *Sp*ChiD.

When the residue Gly-119 was mutated to Ser instead of Trp, the mutant G119S displayed increased TG and decreased hydrolysis [33]. The side chain of Ser-119 had consistent electrostatic interactions with the catalytic residues of D*X*D*X*E motif throughout the 50 ns MD simulations. SIE calculations revealed that Ser-119 had much less vdW and coulomb energy contributions in comparison to *Sp*ChiD–DP4 complex, suggesting decreased interactions with DP4 substrate. The weak interactions of DP4 substrate with Ser-119 and a minor increase in vdW and coulombic energies of the Gly-201 suggested a favored movement of DP4 substrate towards the tunnel exit. The void left unfilled at the tunnel entrance of mutant G119S was greater when compared to the mutant G119W, which will allow the substrate DP4 to enter the active site and expression of hydrolytic and TG activities. DP4 exhibited a decrease in the average number of hydrogen bonds with the mutant G119S when compared to G119W. The stable RMSD

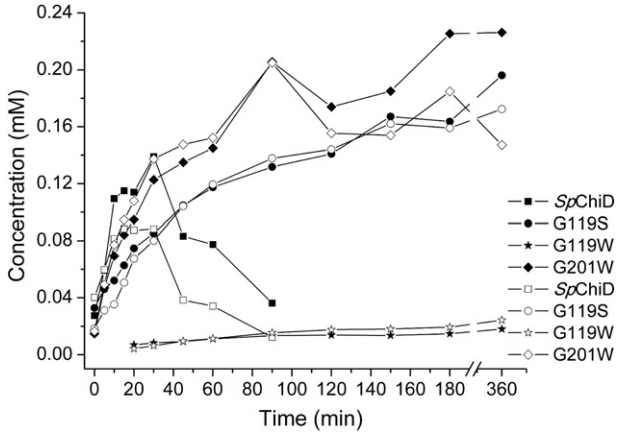

Fig. 6. Comparison of quantifiable TG products. DP5 (solid symbols) and DP6 (hollow symbols) accumulated at different time intervals upon incubation of 2 mM DP4 with *Sp*ChiD and its variants G119S, G119W and G201W. Reaction was carried up to 6 h, pH 5.6, at 40 °C. Product quantification was done by a linear correlation between peak area and concentration of oligosaccharides in standard samples.

(~0.25 nm) of DP4 along with active site of G119S indicated a free movement of DP4 that helps in hydrolysis and TG activities. The mutant G119S also produced nearly similar quantities of TG products DP5 and DP6 up to 6 h (Fig. 6). But, the concentration of TG products produced in the early phase of reaction was less compared to *Sp*ChiD. DP5 concentration was low up to 60 min, whereas, DP6 concentration was low up to 30 min when compared to *Sp*ChiD. The concentration of TG products was increased slowly up to 120 min and a considerable hike was observed at 150 min [33].

The residue Trp-120, adjacent to Gly-119, is an important aromatic residue which maintains the architecture of the catalytic groove and also controls the threading of chitin molecules towards the catalytic center [27,33]. The decreased vdW and coulomb energy for the Ala-120 residue indicates that the Ala side chain showed decreased interactions with DP4. The less favorable interactions observed for the Ala-120 and Gly-119 with DP4 and minor increase in interactions for Gly-201 suggest that the movement of DP4 is towards the tunnel exit. Tunnel entrance of the mutant W120A showed a lot of empty space available because of which the substrate molecules can enter freely and reach the active site. The trafficking of water molecules also increased through the entrance and this could be the main reason for increased hydrolysis with the concomitant loss of TG activity [27,33]. The architecture of the tunnel exit remained undisturbed. The RMSD of DP4 substrate (~0.12 nm) in the groove of the W120A mutant indicates that the stability of substrate is high compared to the overall protein RMSD (~0.4 nm). The relative average number of hydrogen bonds is similar for the DP4 as that of *Sp*ChiD.

The residue Gly-201 corresponds to the +2 subsite of *Sp*ChiD and its mutation to Trp resulted in increased TG. The mutant residue Trp-201 was observed in the region of tunnel exit and its side chain is partially closing the exit. DP4 experienced increased vdW and coulomb interactions with Trp-201 and decreased interactions with the residues Gly-119 and Trp-120. The RMSD (~0.22 nm) of DP4 in the active site converged throughout the MD simulations and the increased average number of hydrogen bonds for G201W shows the affinity for the substrate. The increased TG could be, either due to the high affinity of substrate to the bulky side chain of Trp-201, or may be the introduction of a hydrophobic patch (*i.e.* preventing the entry of a water molecule that would favor hydrolysis). This may further be translated into increased retention time of either the intermediate oxazoline or the substrate DP4 at the active site and thus favoring TG. The mutant G201W produced more of TG products from the early time of reaction with a sudden hike in the concentration of DP5 and DP6 was observed at 90 min (Fig. 6). The TG products were more up to 6 h by G201W, when compared to *Sp*ChiD and the three single mutants (G119S, G119W and W120A). The mutant G201W thus displayed increased TG among all the three Gly variants reported in the present study. Increase of TG activity by partial blocking of the tunnel exit, for family 18 GHs like *Sp*ChiD has hitherto not been reported.

5. Conclusion

Amino acid alterations at the substrate entry and product exit points of the enzyme *Sp*ChiD were studied in detail using MD simulations, SIE free energy changes and HLPC analysis with DP4 as the substrate. The present study provides insights into the structural and dynamic features of *Sp*ChiD a family 18 chitinase with TG activity. The efficiency of TG by the wild-type enzyme is inevitably limited by enzyme-catalyzed hydrolysis of the product [66]. So, there is a definite need for reducing/curtailing the hydrolytic activity for improving TG activity, to generate longer chain CHOS with immense potential for various biological activities.

Supporting information

DP4 binding free energies with *Sp*ChiD and its mutants (Supplementary Table 1). Specific activity of mutants G119W and G201W towards DP4 (Supplementary Fig. 1). The root mean square deviation (RMSD) plots from 50,000 ps MD simulations of DP4 in complex with A) *Sp*ChiD B) G119S C) G119W and D) G201W (Supplementary Fig. 2). RMSD plot for 'apo' form of *Sp*ChiD crystal structure (Supplementary Fig. 3). Superimposition of 10 structures taken at every 5 ns interval of *Sp*ChiD crystal structure (Supplementary Fig. 4). HRMS data was included after Supplementary Fig. 2. This material is available free of charge *via* the Internet at http://pubs.acs.org.

Funding

We thank the Department of Biotechnology, Government of India for a major research grant no: BT/PR5800/PID/6/681/2012 to ARP. We also thank the International Research and Training Group on "Molecular and Cellular Glycosciences" between the University of Hyderabad and the University of Munster. JM and KT thank CSIR, Govt. of India for Senior Research Fellowship.

Acknowledgments

We thank the Department of Science and Technology, Government of India, Funds for Infrastructure in Science and Technology, Level II support to the Department of Plant Sciences and School of Chemistry at the University of Hyderabad. We gratefully acknowledge the support from University Grants Commission (UGC) in the form of Centre for Advanced Studies in Life Sciences and Centre for Advanced Studies in Chemistry. We thank the Department Biotechnology, Government of India, Centre for Research and Education in Biology and Biotechnology to the School of Life Sciences. We also thank UGC-supported University with Potential for Excellence (Phase II) to the University of Hyderabad for the infrastructural support. We thank Center for Modeling Simulation and Design for the computational facilities.

References

[1] B. Henrissat, G. Davies, Structural and sequence-based classification of glycoside hydrolases, Curr. Opin. Struct. Biol. 7 (1997) 637–644.
[2] S. Armand, H. Tomita, A. Heyraud, C. Gey, T. Watanabe, B. Henrissat, Stereochemical course of the hydrolysis reaction catalyzed by chitinases A1 and D from *Bacillus circulans* WL-12, FEBS Lett. 343 (1994) 177–180.
[3] A.C. Terwisscha van Scheltinga, M. Hennig, B.W. Dijkstra, The 1.8 A˚ resolution structure of hevamine, a plant chitinase/lysozyme, and analysis of the conserved sequence and structure motifs of glycosyl hydrolase family 18, J. Mol. Biol. 262 (1996) 243–257.

[4] A. Perrakis, I. Tews, Z. Dauter, A.B. Oppenheim, I. Chet, K.S. Wilson, C.E. Vorgias, Crystal structure of a bacterial chitinase at 2.3 Å resolution, Structure 2 (1994) 1169–1180.

[5] A.C. Terwisscha van Scheltinga, K.H. Kalk, J.J. Beintema, B.W. Dijkstra, Crystal structures of hevamine, a plant defence protein with chitinase and lysozyme activity, and its complex with an inhibitor, Structure 2 (1994) 1181–1189.

[6] T. Hollis, A.F. Monzingo, K. Bortone, S. Ernst, R. Cox, J.D. Robertus, The X-ray structure of a chitinase from the pathogenic fungus *Coccidioides immitis*, Protein Sci. 9 (2000) 544–551.

[7] D.M. van Aalten, B. Synstad, M.B. Brurberg, E. Hough, B.W. Riise, V.G.H. Eijsink, R.K. Wierenga, Structure of a two-domain chitotriosidase from *Serratia marcescens* at 1.9 Å resolution, Proc. Natl. Acad. Sci. U. S. A. 97 (2000) 5842–5847.

[8] F. Fusetti, H. von Moeller, D. Houston, H.J. Rozeboom, B.W. Dijkstra, R.G. Boot, J.M.F. G. Aerts, D.M.F. van Aalten, Structure of human chitotriosidase. Implications for specific inhibitor design and function of mammalian chitinase-like lectins, J. Biol. Chem. 277 (2002) 25537–25544.

[9] I. Tews, A.C.T. van Scheltinga, A. Perrakis, K.S. Wilson, B.W. Dijkstra, Substrate-assisted catalysis unifies two families of chitinolytic enzymes, J. Am. Chem. Soc. 119 (1997) 7954–7959.

[10] D.M.F. van Aalten, D. Komander, B. Synstad, S. Gaseidnes, M.G. Peter, V.G.H. Eijsink, Structural insights into the catalytic mechanism of a family 18 exo-chitinase, Proc. Natl. Acad. Sci. U. S. A. 98 (2001) 8979–8984.

[11] D.W. Abbott, M.S. Macauley, D.J. Vocadlo, A.B. Boraston, *Streptococcus pneumonia* endohexosaminidase D, structural and mechanistic insight into substrate-assisted catalysis in family 85 glycoside hydrolases, J. Biol. Chem. 284 (2009) 11676–11689.

[12] B.L. Mark, D.J. Vocadlo, S. Knapp, B.L. Triggs-Raine, S.G. Withers, M.N. James, Crystallographic evidence for substrate-assisted catalysis in a bacterial β-hexosaminidase, J. Biol. Chem. 276 (2001) 10330–10337.

[13] B. Synstad, S. Gaseidnes, D.M.F. van Aalten, G. Vriend, J.E. Nielsen, V.G.H. Eijsink, Mutational and computational analysis of the role of conserved residues in the active site of a family 18 chitinase, Eur. J. Biochem. 271 (2004) 253–262.

[14] T. Uchiyama, F. Katouno, N. Nikaidou, T. Nonaka, J. Sugiy-ama, T. Watanabe, Roles of the exposed aromatic residues in crystalline chitin hydrolysis by chitinase A from *Serratia marcescens* 2170, J. Biol. Chem. 276 (2001) 41343–41349.

[15] C.M. Payne, J. Baban, S.J. Horn, P.H. Backe, A.S. Arvai, B. Dalhus, M. Bjørås, V.G. Eijsink, M. Sørlie, G.T. Beckham, G. Vaaje-Kolstad, Hallmarks of processivity in glycoside hydrolases from crystallographic and computational studies of the *Serratia marcescens* chitinases, J. Biol. Chem. 287 (2012) 36322–36330.

[16] M. Rinaudo, Chitin and chitosan. Properties and applications, Prog. Polym. Sci. 31 (2006) 603–632.

[17] R.N. Tharanathan, F.S. Kittur, Chitin. The undisputed biomolecule of great potential, Crit. Rev. Food Sci. Nutr. 43 (2003) 61–87.

[18] Y.J. Jeon, P.J. Park, S.K. Kim, Antimicrobial effect of chitooligosaccharides produced by bioreactor, Carbohydr. Polym. 44 (2001) 71–76.

[19] K.V.H. Prashanth, R.N. Tharanathan, Depolymerized products of chitosan as potent inhibitors of tumor-induced angiogenesis, Biochim. Biophys. Acta 1722 (2005) 22–29.

[20] J.G. Xu, X.M. Zhao, X.W. Han, Y.G. Du, Antifungal activity of oligo-chitosan against *Phytophthora capsici* and other plant pathogenic fungi *in vitro*, Pestic. Biochem. Physiol. 87 (2007) 220–228.

[21] H.T. Liu, W.M. Li, G. Xu, X.Y. Li, X.F. Bai, P. Wei, C. Yu, Y.G. Du, Chitosan oligosaccharides attenuate hydrogen peroxide induced stress injury in human umbilical vein endothelial cells, Pharmacol. Res. 59 (2009) 167–175.

[22] D.N. Ngo, M.M. Kim, S.K. Kim, Chitin oligosaccharides inhibit oxidative stress in live cells, Carbohydr. Polym. 74 (2008) 228–234.

[23] F.L. Fonseca, L. Nimrichter, R.J. Cordero, S. Frases, J. Rodrigues, D.L. Goldman, R. Andruszkiewicz, S. Milewski, L.R. Travassos, A. Casadevall, M.L. Rodrigues, Role for chitin and chitooligomers in the capsular architecture of *Cryptococcus neoformans*, Eukaryot. Cell 8 (2009) 1543–1553.

[24] F.L. Fonseca, A.J. Guimarães, L. Kmetzsch, F.F. Dutra, F.D. Silva, C.P. Taborda, S. Araujo Gde, S. Frases, C.C. Staats, M.T. Bozza, A. Schrank, M.H. Vainstein, L. Nimrichter, A. Casadevall, M.L. Rodrigues, Binding of the wheat germ lectin to *Cryptococcus neoformans* chitooligomers affects multiple mechanisms required for fungal pathogenesis, Fungal Genet. Biol. 60 (2013) 64–73.

[25] L.P. Hamel, N. Beaudoin, Chitooligosaccharide sensing and down-stream signaling. Contrasted outcomes in pathogenic and beneficial plant-microbe interactions, Planta 232 (2010) 787–806.

[26] P. Purushotham, A.R. Podile, Synthesis of long-chain chitooligosaccharides by a hypertransglycosylating processive endochitinase of *Serratia proteamaculans* 568, J. Bacteriol. 194 (2012) 4260–4271.

[27] H. Zakariassen, M.C. Hansen, M. Jøranli, V.G.H. Eijsink, M. Sørlie, Mutational effects on transglycosylating activity of family 18 chitinases and construction of a hypertransglycosylating mutant, Biochemistry 50 (2011) 5693–5703.

[28] M. Umekawa, W. Huang, B. Li, K. Fujita, H. Ashida, L.X. Wang, K. Yamamoto, Mutants of *Mucor hiemalis* endo-β-N-acetylglucosaminidase show enhanced transglycosylation and glycosynthase-like activities, J. Biol. Chem. 283 (2008) 4469–4479.

[29] H.D. Ly, S.G. Withers, Mutagenesis of glycosidases, Annu. Rev. Biochem. 68 (1999) 487–522.

[30] S.N. Das, J. Madhuprakash, P.V.S.R.N. Sarma, P. Purushotham, K. Suma, K. Manjeet, S. Rambabu, N.E. El Gueddari, B.M. Moerschbacher, A.R. Podile, Biotechnological approaches for field applications of chitooligosaccharides (COS) to induce immunity in plants, Crit. Rev. Biotechnol. (2013), http://dx.doi.org/10.3109/07388551.2013.798255.

[31] T. Fukamizo, S. Goto, T. Torikata, T. Araki, Enhancement of transglycosylation activity of lysozyme by chemical modification, Agric. Biol. Chem. 53 (1989) 2641–2651.

[32] N.N. Aronson Jr., B.A. Halloran, M.F. Alexeyev, X.E. Zhou, Y. Wang, E.J. Meehan, L. Chen, Mutation of a conserved tryptophan in the chitin-binding cleft of *Serratia marcescens* chitinase A enhances transglycosylation, Biosci. Biotechnol. Biochem. 70 (2006) 243–251.

[33] J. Madhuprakash, K. Tanneeru, P. Purushotham, L. Guru Prasad, A.R. Podile, Transglycosylation by chitinase D from *Serratia proteamaculans* improved through altered substrate interactions, J. Biol. Chem. 287 (2012) 44619–44627.

[34] T. Taira, M. Fujiwara, N. Dennhart, H. Hayashi, S. Onaga, T. Ohnuma, T. Letzel, S. Sakuda, T. Fukamizo, Transglycosylation reaction catalyzed by a class V chitinase from cycad, *Cycas revoluta*. A study involving site-directed mutagenesis, HPLC, and real time ESI-MS, Biochim. Biophys. Acta 1804 (2010) 668–675.

[35] N. Umemoto, T. Ohnuma, M. Mizuhara, H. Sato, K. Skriver, T. Fukamizo, Introduction of a tryptophan side chain into subsite +1 enhances transglycosylation activity of a GH-18 chitinase from *Arabidopsis thaliana*, AtChiC, Glycobiology 23 (2013) 81–90.

[36] S.H. Ke, E.L. Madison, Rapid and efficient site-directed mutagenesis by single-tube "megaprimer" PCR method, Nucleic Acids Res. 25 (1997) 3371–3372.

[37] C. Neeraja, B. Moerschbacher, A.R. Podile, Fusion of cellulose binding domain to the catalytic domain improves the activity and conformational stability of chitinase in *Bacillus licheniformis* DSM13, Bioresour. Technol. 101 (2010) 3635–3641.

[38] J. Madhuprakash, A. Singh, S. Kumar, M. Sinha, P. Kaur, S. Sharma, A.R. Podile, T.P. Singh, Structure of chitinase D from *Serratia proteamaculans* reveals the structural basis of its dual action of hydrolysis and transglycosylation, Int. J. Biochem. Mol. Biol. 4 (2013) 166–178.

[39] J. Wang, R.M. Wolf, J.W. Caldwell, P.A. Kollman, D.A. Case, Development and testing of a general amber force field, J. Comput. Chem. 25 (2004) 1157–1174.

[40] J. Wang, W. Wang, P.A. Kollman, D.A. Case, Automatic atom type and bond type perception in molecular mechanical calculations, J. Mol. Graph. Model. 25 (2006) 247–260.

[41] A.W. Sousa da Silva, W.F. Vranken, ACPYPE — AnteChamber PYthon Parser interfacE, BMC Res. Notes 5 (2012) 367.

[42] B. Hess, C. Kutzner, D. van der Spoel, E. Lindahl, GROMACS 4. Algorithms for highly efficient, load-balanced and scalable molecular simulation, J. Chem. Theory Comput. 4 (2008) 435–447.

[43] D. van der Spoel, E. Lindahl, B. Hess, G. Groenhof, A.E. Mark, H.J.C. Berendsen, GROMACS. Fast, flexible and free, J. Comput. Chem. 26 (2005) 1701–1718.

[44] T. Darden, D. York, L. Pedersen, Particle Mesh Ewald: an N log (N) method for Ewald sums in large systems, J. Chem. Phys. 98 (1993) 10089–10092.

[45] U. Essmann, L. Perera, M.L. Berkowitz, T. Darden, H. Lee, L.G. Pedersen, A smooth Particle Mesh Ewald method, J. Chem. Phys. 103 (1995) 8577–8593.

[46] G. Bussi, D. Donadio, M. Parrinello, Canonical sampling through velocity-rescaling, J. Chem. Phys. 126 (2007) 014101.

[47] M. Parrinello, A. Rahman, Polymorphic transitions in single crystals. A new molecular dynamics method, J. Appl. Phys. 52 (1981) 7182–7190.

[48] B. Hess, H. Bekker, H.J.C. Berendsen, J.G.E.M. Fraaije, LINCS. A linear constraint solver for molecular simulations, J. Comput. Chem. 18 (1997) 1463–1472.

[49] M. Naïm, S. Bhat, K.N. Rankin, S. Dennis, S.F. Chowdhury, I. Siddiqi, P. Drabik, T. Sulea, C.I. Bayly, A. Jakalian, E.O. Purisima, Solvated interaction energy (SIE) for scoring protein-ligand binding affinities. 1. Exploring the parameter space, J. Chem. Inf. Model. 47 (2007) 122–133.

[50] T. Sulea, Q. Cui, E.O. Purisima, Solvated interaction energy (SIE) for scoring protein-ligand binding affinities. 2. Benchmark in the CSAR-2010 scoring exercise, J. Chem. Inf. Model. 51 (2011) 2066–2681.

[51] X. Zou, Y. Sun, I.D. Kuntz, Inclusion of solvation in ligand binding free energy calculations using the generalized-born model, J. Am. Chem. Soc. 121 (1999) 8033–8043.

[52] P.A. Kollman, I. Massova, C. Reyes, B. Kuhn, S. Huo, L. Chong, M. Lee, T. Lee, Y. Duan, W. Wang, O. Donini, P. Cieplak, J. Srinivasan, D.A. Case, T.E. Cheatham, Calculating structures and free energies of complex molecules. Combining molecular mechanics and continuum models, Acc. Chem. Res. 33 (2000) 889–897.

[53] B. Kuhn, P. Gerber, T. Schulz-Gasch, M. Stahl, Validation and use of the MM-PBSA approach for drug discovery, J. Med. Chem. 48 (2005) 4040–4048.

[54] H. Gohlke, D.A. Case, Converging free energy estimates. MM-PB (GB) SA studies on the protein–protein complex Ras–Raf, J. Comput. Chem. 25 (2004) 238–250.

[55] J. Aqvist, V.B. Luzhkov, B.O. Brandsdal, Ligand binding affinities from MD simulations, Acc. Chem. Res. 35 (2002) 358–365.

[56] Q. Cui, T. Sulea, J.D. Schrag, C. Munger, M.N. Hung, M. Naim, M. Cygler, E.O. Purisima, Molecular dynamics-solvated interaction energy studies of protein-protein interactions: the MP1-p14 scaffolding complex, J. Mol. Biol. 379 (2008) 787–802.

[57] E.O. Purisima, S.H. Nilar, A simple yet accurate boundary-element method for continuum dielectric calculations, J. Comput. Chem. 16 (1995) 681–689.

[58] E.O. Purisima, Fast summation boundary element method for calculating solvation free energies of macromolecules, J. Comput. Chem. 19 (1998) 1494–1504.

[59] M.A. Lill, J.J. Thompson, Solvent interaction energy calculations on molecular dynamics trajectories: increasing the efficiency using systematic frame selection, J. Chem. Inf. Model. 51 (2011) 2680–2689.

[60] W. Chen, C.E. Chang, M.K. Gilson, Calculation of cyclodextrin binding affinities. Energy, entropy, and implications for drug design, Biophys. J. 87 (2004) 3035–3049.

[61] C.M. Payne, Y.J. Bomble, C.B. Taylor, C. McCabe, M.E. Himmel, M.F. Crowley, G.T. Beckham, Multiple functions of aromatic carbohydrate interactions in a processive cellulase examined with molecular simulation, J. Biol. Chem. 286 (2011) 41028–41035.

[62] D.M.F. van Aalten, B. Synstad, M.B. Brurberg, E. Hough, B.W. Riise, V.G.H. Eijsink, R.K. Wierenga, Structure of a two-domain chitotriosidase from *Serratia marcescens* at 1.9 Å resolution, Proc. Natl. Acad. Sci. U. S. A. 97 (2000) 5842–5847.

[63] K. Suzuki, N. Sugawara, M. Suzuki, T. Uchiyama, F. Katouno, N. Nikaidou, T. Watanabe, Chitinases A, B, and C1 of *Serratia marcescens* 2170 produced by recombinant *Escherichia coli*: enzymatic properties and synergism on chitin degradation, Biosci. Biotechnol. Biochem. 66 (2002) 1075–1083.

[64] S.J. Horn, A. Sørbotten, B. Synstad, P. Sikorski, M. Sørlie, K.M. Vårum, V.G. Eijsink, Endo/exo mechanism and processivity of family 18 chitinases produced by *Serratia marcescens*, FEBS J. 273 (2006) 491–503.
[65] E.L. Hult, F. Katouno, T. Uchiyama, T. Watanabe, J. Sugiyama, Molecular directionality in crystalline-chitin: hydrolysis by chitinases A and B from *Serratia marcescens* 2170, Biochem. J. 388 (2005) 851–856.
[66] Z. Ling, M.D. Suits, R.J. Bingham, N.C. Bruce, G.J. Davies, A.J. Fairbanks, J.W. Moir, E.J. Taylor, The X-ray crystal structure of an *Arthrobacter protophormiae* endo-β-N-acetylglucosaminidase reveals a $(\beta/\alpha)_8$ catalytic domain, two ancillary domains and active site residues key for transglycosylation activity, J. Mol. Biol. 389 (2009) 1–9.
[67] H. Zakariassen, B.B. Aam, S.J. Horn, K.M. Vårum, M. Sørlie, V.G. Eijsink, Aromatic residues in the catalytic center of chitinase A from *Serratia marcescens* affect processivity, enzyme activity, and biomass converting efficiency, J. Biol. Chem. 284 (2009) 10610–10617.
[68] T. Watanabe, Y. Ariga, U. Sato, T. Toratani, M. Hashimoto, N. Nikaidou, Y. Kezuka, T. Nonaka, J. Sugiyama, Aromatic residues within the substrate-binding cleft of *Bacillus circulans* chitinase A1 are essential for hydrolysis of crystalline chitin, Biochem. J. 376 (2003) 237–244.